A Combined Applied Mechanics/Materials Science Approach Toward Quantifying the Role of Hydrogen on Material Degradation

P. Sofronis[1], M. Dadfarnia[1], P. Novak[1], R. Yuan[2], B. Somerday[3], I.M. Robertson[1], R.O. Ritchie[2], T. Kanezaki[4], Y. Murakami[4]

[1]*University of Illinois at Urbana-Champaign, Urbana, USA;* [2]*University of California, Berkeley, USA;* [3]*Sandia National Laboratories, Livermore, USA;* [4]*Kyushu University, Fukuoka, Japan*

Abstract:

Development and validation of a lifetime prediction methodology for failure of materials used for hydrogen containment components is of paramount importance to the planned hydrogen economy. In the case of low strength steel pipelines, we outline a hydrogen transport methodology for the calculation of hydrogen accumulation ahead of the tip of an axial crack on the inner surface. For all practical purposes, we find that the stress, deformation, and hydrogen fields exhibit a small scale character which allows for the use of the standard modified boundary layer approach to the study of the fracture behavior of steel pipelines. Arguably the most devastating mode of hydrogen-induced degradation is the hydrogen embrittlement of high-strength steels. We present an approach to quantify the effect of hydrogen on the fracture strength and toughness of a low alloy martensitic steel through the use of a statistically-based micromechanical model for the critical local fracture event.

1. Introduction:

Hydrogen embrittlement is a severe environmental type of failure [1]. When hydrogen is present, materials fail at load levels that are very low compared with those that a hydrogen free material can sustain. Of the many suggestions, three are the mechanisms of embrittlement that appear to be viable: stress-induced hydride formation and cleavage [2], hydrogen-enhanced localized plasticity (HELP) [3], and hydrogen-induced decohesion [4]. Despite the fact that these degradation mechanisms are well understood, no models of hydrogen-induced fracture that are based on the interaction of hydrogen with the material microstructure are available. In this paper we attempt to characterize the relationship of this interaction with indices of failure such as the stress intensity factor or the macroscopic fracture load for a notched specimen. We focus attention on steels which are material systems that do not form hydrides. We demonstrate that low strength steels, which are under consideration for use as hydrogen transporting pipeline materials, can be characterized both mechanically and environmentally through a constraint fracture mechanics approach [5]. For components made of high strength steels, we propose a model of decohesion-induced failure that links the microstructural decohesion event with the macroscopic load.

2. Hydrogen Diffusion in an Elastoplastically Deforming Material

We assume that hydrogen either diffuses through normal interstitial lattice sites (NILS) or gets trapped at trapping sites at microstructural defects such as internal interfaces or dislocations generated by plastic deformation [6]. According to Oriani's theory [7] the two populations are assumed to be in equilibrium such that $\theta_T/(1-\theta_T)=\theta_L/(1-\theta_L)\exp(W_B/R\Theta)$ where θ_L is the occupancy of the interstitial sites, θ_T is the occupancy of the trapping sites, W_B is the trap binding energy, R = 8.314 J/mol K is the universal gas constant, and Θ is the absolute temperature. The hydrogen concentration in trapping sites C_T, measured in hydrogen atoms per unit volume, can be written as $C_T=\theta_T\alpha N_T$, where α denotes the number of sites per trap, and N_T denotes the number of traps per unit volume which can be a function of the local plastic straining. Similarly, the hydrogen concentration in interstitial sites C_L, measured in hydrogen atoms per unit volume, can be phrased as $C_L=\theta_L\beta N_L$, where β denotes the number of NILS per solvent atom, N_L denotes the number of solvent atoms per unit volume given by $N_L=N_A/V_M$ with $N_A=6.0232\times10^{23}$ atoms per mole being Avogadro's number, and V_M is the molar volume of the host lattice measured in units of volume per mole.

The transient diffusion of hydrogen accounting for trapping and hydrostatic stress drift can be expressed as [6,8]

$$\frac{D}{D_{eff}}\frac{dC_L}{dt}+\alpha\theta_T\frac{dN_T}{d\varepsilon^p}\frac{d\varepsilon^p}{dt}-DC_{L,ii}+\left(\frac{DV_H}{3R\Theta}C_L\sigma_{kk,i}\right)_{,i}=0, \qquad (1)$$

where $()_{,i}=\partial()/\partial x_i$, d/dt is the time derivative, D is the hydrogen diffusion coefficient through NILS, $D_{eff}=D/\left(1+\partial C_T/\partial C_L\right)$ is an effective diffusion coefficient reflecting the presence of traps, V_H is the partial molar volume of hydrogen in solid solution, σ_{ij} is the Cauchy stress, and a repeated index implies the standard summation convention over the range.

Equation (1) shows that in order to calculate the hydrogen distribution within a solid, one needs to solve the coupled problem of hydrogen diffusion and material elastoplastic deformation [6]. The finite element procedures for the solution of the coupled problems are outlined in the works by Sofronis and McMeeking [6].

3. Low Strength Pipeline Steel for Hydrogen Gas Delivery

We study the hydrogen interaction with material elastoplasticity at an axial crack on the inner diameter (ID) surface of a pipe i) by solving the coupled problem over the domain of an actual pipe [9] and ii) through a boundary layer formulation under Mode I loading and small scale yielding (SSY) conditions [9,10]. We term

the former approach full-field solution as it pertains to the specific pipe dimensions and the latter one modified boundary layer (MBL) formulation. Lastly, we compare the results from both approaches.

3.1 Full field solution

We analyze the mechanics of hydrogen uptake through the surfaces of an axial crack on the ID surface of a pipe by solving the coupled hydrogen transport/elastoplasticity problem over the entire cross-sectional area of the pipe. The applied hydrogen pressure on the ID surface as well as on the crack faces opens up the crack and forces hydrogen to diffuse through the pipeline wall. Figure 1 describes the hydrogen-related boundary and initial conditions of the problem in the full-field formulation. Due to symmetry, we consider only half the pipeline cross-sectional area. The pipeline wall material is initially hydrogen-free and all surfaces in contact with hydrogen (ID surface and crack faces) at time $t \geq 0$ are at equilibrium with the hydrogen gas pressure in the pipe as dictated by Sievert's law. The outer diameter (OD) surface of the pipeline is maintained at zero hydrogen concentration ($C_L = 0$) simulating hydrogen outgassing or insulated ($j = 0$) for the case of an OD surface that is coated or has formed an oxide. Also, the hydrogen flux is zero at the plane of symmetry.

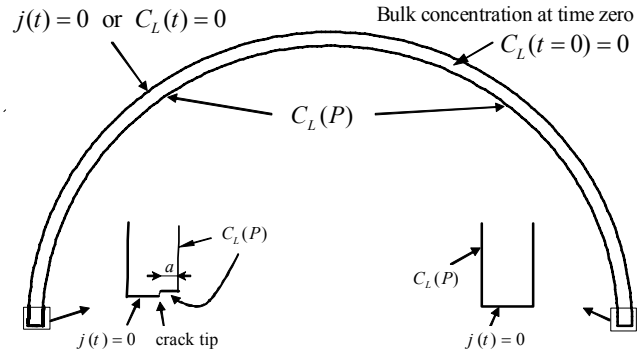

Figure 1. Description of the initial and boundary conditions for the hydrogen diffusion problem in the pipe. The parameter *j* denotes hydrogen flux and $C_L(P)$ is normal interstitial lattice site hydrogen concentration at the ID surface of the pipe in equilibrium with the hydrogen gas pressure *P* as it increases to 15 MPa in 1 sec. At time zero, the material is hydrogen free, $C_L(t = 0) = 0$.

For the numerical calculations, we considered the material properties of a new X70/X80 type of an acicular ferrite pipeline microstructure. The uniaxial stress-strain curve of this steel has been determined experimentally and is described by $\sigma_e = \sigma_0(1 + \varepsilon^p / \varepsilon_0)^n$, where ε^p is the plastic strain, σ_0 = 595 MPa is the yield stress, $\varepsilon_0 = \sigma_0 / E$ the yield strain, and n = 0.059 the work hardening exponent. The Poisson's ratio is ν=0.3 and Young's modulus E=201.88 GPa. The system's temperature is Θ = 300 K. We assume the hydrogen lattice diffusion coefficient at this temperature to be $D = 1.271 \times 10^{-8}$ m^2/s [1]. The partial molar volume of

hydrogen in solid solution is $V_H = 2\times10^{-6}\,\mathrm{m}^3/\mathrm{mol}$ [1] and the solubility 0.005435 mol $H_2/m^3\sqrt{MPa}$. The molar volume of the material is 7.116×10^{-6} m^3/mol. We set the parameters β and α equal to 1. For the trap density N_T, we assumed that it increases with plastic strain according to the experimental results of Kumnick and Johnson [11]. These investigators also found a trap binding energy of 60 kJ/mol.

We carried out the numerical simulations for a pipe with an OD equal to 40.64 cm, wall thickness h = 9.52 mm and an axial crack of depth a = 0.476 mm (a/h = 0.05). Hydrogen diffusion begins at time $t > 0$ as the hydrogen pressure is increased to 15 MPa over 1 sec and then kept constant at 15 MPa. At this pressure, the corresponding crack tip opening displacement (CTOD) b is equal to 1.17 μm, which is about 4 times the assumed initial CTOD b_0 = 0.3 μm. On the ID surface and the crack faces, the NILS hydrogen concentration C_L is maintained at equilibrium with the hydrogen gas in the pipe. At 15 MPa and temperature Θ = 300 K., this concentration is equal to $C_0 = 2.659\times10^{22}$ H atoms/m^3 (=3.142×10^{-7} H atoms per solvent atoms).

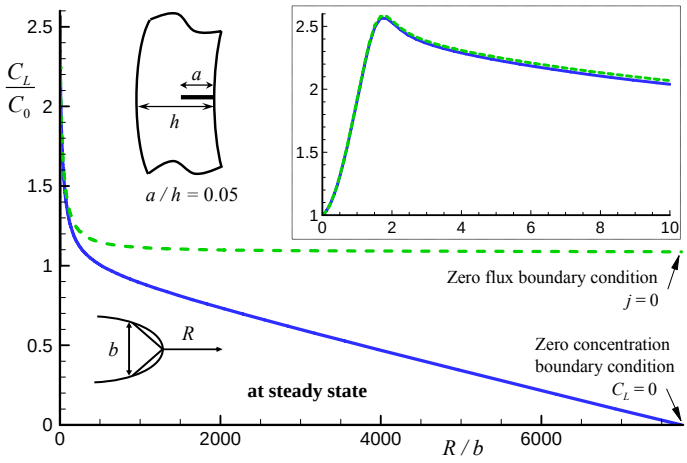

Figure 2. Steady state normalized NILS hydrogen concentration C_L/C_0 vs. normalized distance R/b from the crack tip for the full-field solution over the entire uncracked ligament under different boundary conditions on the OD surface of the pipe. The inset shows the concentrations near the crack tip.

Figure 2 shows the full-field steady state normalized NILS hydrogen concentration ahead of the crack tip as obtained for the two cases of boundary conditions on the OD surface. Although the values of the hydrogen concentration on the outer boundary (OD surface) for the two cases are markedly different, the profiles of the normalized hydrogen concentration close to the crack tip are identical. This demonstrates that as long as the plasticity in the neighborhood of an axial crack is confined to the crack tip, i.e., small scale yielding conditions prevail, the profile of the hydrogen concentration in the near tip fracture process zone is almost insensitive to the remote boundary condition on the OD surface of the pipe.

3.2 Modified Boundary Layer (MBL) solution

We analyzed the hydrogen transport near the crack tip through a MBL formulation [9] in terms of the stress intensity factor and the *T*-stress that the crack tip experiences in the actual pipe under hydrogen pressure of 15 MPa. The *T*-stress, which influences the hydrostatic constraint ahead of the crack tip in the actual pipe, is the first non-singular constant term in the asymptotic mode I singular elastic solution at a crack tip.

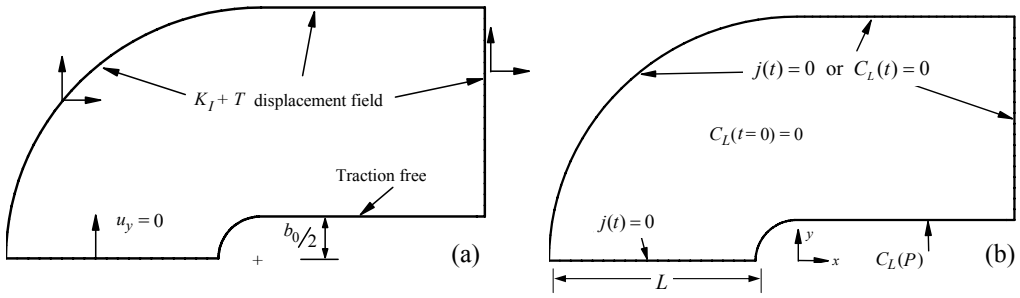

Figure 3. Description of (a) boundary conditions for the elastoplastic problem and (b) initial and boundary conditions for the hydrogen diffusion problem at the blunting crack tip in the MBL formulation. The parameter b_0 denotes the crack tip opening displacement and $C_L(P)$ denotes NILS hydrogen concentration on the crack face in equilibrium with hydrogen gas pressure *P*.

In the MBL approach [9] (Fig. 3) we increase the stress intensity factor and the *T*-stress linearly from zero to $K_I = 14.38$ MPa$\sqrt{\text{m}}$ and $T/\sigma_0 = -0.292$, respectively over 1 sec, and we then keep them constant. These magnitudes of the stress intensity factor K_I and *T*-stress are for the axial crack of depth a = 0.476 mm (a/h = 0.05) in the pipeline we analyzed in section 3.1 at 15 MPa hydrogen pressure. As shown by Fig. 3, we assume that the hydrogen concentration boundary condition on the crack faces is the same as that in the full-field solution approach, and the hydrogen concentration at the outer boundary of the domain is the same as that on the OD surface of the pipeline. We chose the size of the uncracked wall ligament to be the size of the hydrogen transport domain, i.e., $L = h - a$ = 9.049 mm and we took the initial CTOD to be b_0 = 0.3 μm, the same as the initial CTOD we used in the analysis for the actual pipeline.

Next we compare the full-field solution with the solution we obtained using the MBL approach. Although the stress and deformation fields we obtained from the two approaches are different away from the crack tip, the fields close to the crack tip are almost identical [5,9]. The same result also holds for the hydrogen concentration fields [9]. Figure 4 shows the steady-state normalized concentration C_L/C_0 in NILS plotted against normalized distance R/b from the crack tip for both MBL and full-field solutions. There is an excellent agreement between MBL

and full-field solutions for the concentration fields close to the crack tip regardless of the remote concentration boundary condition. In fact, the peak hydrogen concentrations at steady state for all solutions shown differ by at most 1%. This is a very important result for the study and analysis of the fracture response of a pipeline with an axial crack. Having determined the stress intensity factor K_I and the *T*-stress under the given hydrogen pressure, one can use the MBL approach, that is, a laboratory specimen, to calculate in an expedient way the steady state hydrogen concentration profile ahead of the crack tip. If the crack in the laboratory specimen is seen to be stationary for long time, then the combination of K_I, *T*-stress, and hydrogen pressure in the pipeline define safe operation conditions. By repeating this experiment under different pressures a locus for safe-operation conditions can be explored.

We note that although the conclusions drawn above are for an axial crack on the ID surface of a pipe with a specific crack depth $a = 0.05h$, the conclusions continue to be valid for crack depths that ensure SSY conditions at the crack tip [9,12].

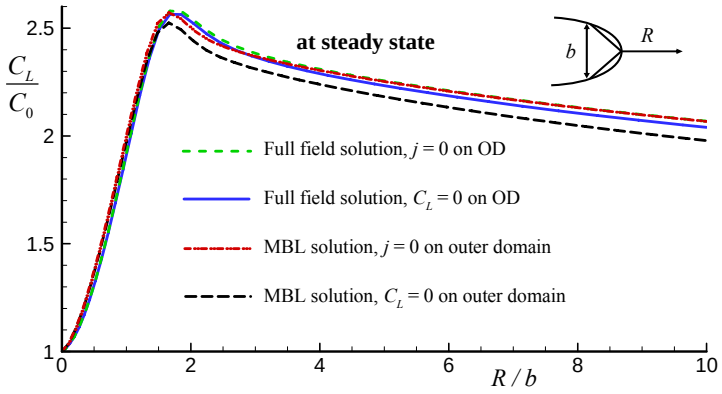

Figure 4. Normalized NILS hydrogen concentration C_L / C_0 near the crack tip at steady state vs. normalized distance *R*/*b* from the crack tip for the full-field (crack depth *a*/*h*=0.05) and MBL solutions under different boundary conditions on the OD surface and outer domain, respectively.

4. Embrittlement of High Strength Steel

Next, we develop a statistical model of fracture for high-strength steels in the presence of hydrogen. High-strength steels in the absence of hydrogen usually fail in a ductile manner whereas hydrogen-charged samples fail by a brittle intergranular mode [1]. Our contention is that hydrogen-induced intergranular failure is triggered by a carbide/matrix interfacial decohesion event brought about by the impingement of a dislocation pile-up onto a carbide particle [13]. The presence of hydrogen reduces the work of interfacial fracture according to the thermodynamic theory of decohesion of Hirth and Rice [14]. We used thermal desorption spectroscopy (TDS) to identify and quantify the types and strengths of the hydrogen trapping sites.

4.1 Statistical Model

We consider decohesion at the carbide/matrix interface and treat the resultant cracks as non-interacting flaws capable of propagating unstably. Thus, we deem that weakest link statistics are applicable [15]. Weakest link statistics dictate that volume elements dV of the material subject to stress σ have a failure probability $\mathrm{d}\phi$

$$d\phi = 1 - \exp\left[-dV\int_0^{\sigma} g(S)\,dS\right] \tag{2}$$

and hence the total survival probability Φ is

$$1 - \Phi = \exp\left[-\int_0^{V}\int_0^{\sigma} g(S)\,dS dV\right], \tag{3}$$

where σ denotes a single component (e.g. maximum principal stress) of the local stress tensor σ_{ij} and $\int_0^{\sigma} g(S)\,dS$ is the fraction of particles per unit volume with interfacial strength less than σ. We find the number of particles with interfacial strength less than σ by relating the carbide size, l, to the strength S through the Smith model [16]

$$\frac{l}{d}S^2 + \tau_{eff}^2\left[1 + \frac{4}{\pi}\frac{\tau_i}{\tau_{eff}}\sqrt{\frac{l}{d}}\right]^2 = \frac{4E\gamma_{eff}}{\pi(1-\nu^2)d}, \tag{4}$$

where d is the grain boundary diameter, τ_i is the friction stress, τ_{eff} is the effective stress which is the difference between the flow stress in shear and the friction stress, $\tau_{eff} = \tau_Y - \tau_i$, and γ_{eff} is the fracture energy of decohesion of the carbide/matrix interface .

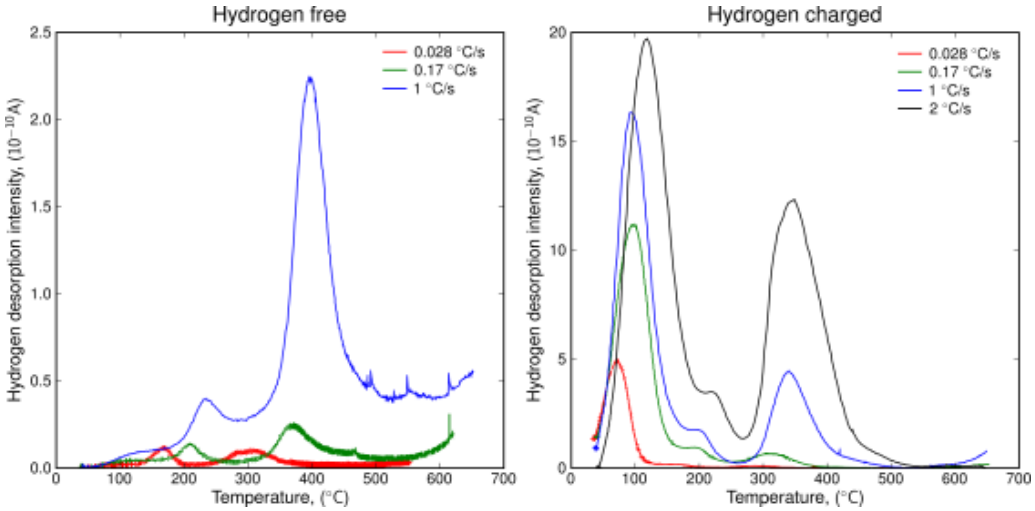

Figure 5. Thermal desorption spectroscopy results show the presence of hydrogen in the nominally hydrogen-free material (left) and the existence of three types of traps, corresponding to the peaks in intensity (right). The temperature at the peak, in conjuction with the heating rate, is used to determine the trap binding energy.

4.2 Thermal Desorption Spectroscopy (TDS)

We performed thermal desorption spectroscopy on high strength AISI 4340 steel samples (heat treated in the austenitized (870ºC, 1 hr), oil quenched, and tempered (200ºC, 2 hr) condition to a R_C hardness of 53), nominally hydrogen-free state, and in the hydrogen-charged state. Figure 5 reveals the existence of three traps of differing binding energies W_B, namely 25, 55, and 79 kJ/mol, corresponding to dislocations, grain boundaries, and carbides [1]. TDS results support the notion that only the diffusible hydrogen through the lattice sites or the hydrogen residing at the traps with the lowest binding energy contributes to material embrittlement; the deeper traps were saturated in both hydrogen free and charged samples.

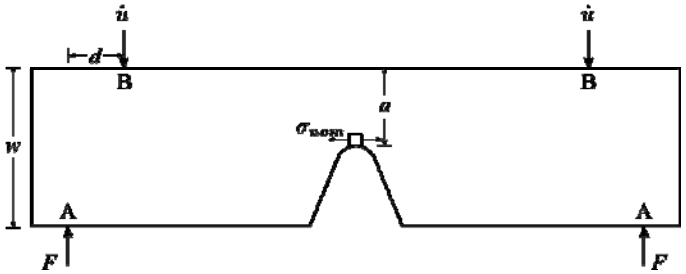

Figure 6. Schematic of SEN specimen, which was hydrogen charged to an initial concentration of C_L^0 and loaded under displacement control at points B. The failure load is given in terms of the nominal stress $\sigma_{nom} = 6Fd / wa^2$, the maximum stress in a un-notched beam of height a. The specimens were tested in air, so zero concentration boundary conditions were assumed.

4.3 Results

We charged single-edge notch (SEN) AISI 4340 steel specimens in hydrogen gas for two weeks. We found the failure loads by loading the specimens in four point bending (Fig. 6) until fracture. We determined the probability of failure by performing finite element analysis of the hydrogen redistribution during loading and calculating the hydrogen effect on the fracture work γ_{eff} via the Hirth and Rice [14] thermodynamic model of decohesion [17]. Specifically, the uniaxial stress-strain curve of this steel is described by $\sigma_e = \sigma_0(1+\varepsilon^p / \varepsilon_0)^n$, where σ_0 = 1490 MPa, n = 0.13, $\varepsilon_0 = \sigma_0 / E$, and E = 200 GPa. The hydrogen concentration field during loading is determined by Eq. (1), modified to admit the presence of three types of traps; the density of the shallowest traps evolves with plastic strain as described in Section 3.1. The other two trap densities are constant at $N_{T2} = 10^{21}$ m^{-3} [1] for grain boundaries and $N_{T3} = 6\times10^{12}$ m^{-3} for carbides. The carbide size l ranges from 0.1 to 2 μm, the grain diameter $d = 10\,\mu$m, and the friction stress is taken approximately equal to $10^{-3}\mu$, where μ is the shear modulus. The fracture work γ_{eff}, in the absence of hydrogen, is 23 J/m^2 [15] and reduces in the presence of hydrogen [17].

The combination of the Hirth-Rice thermodynamic theory of decohesion and the statistical model of fracture predicts accurately the failure loads for 4340 steel (Fig. 7) as a function of the hydrogen concentration in the stress-free state. By knowing the sizes of the carbide particles distributed throughout the steel and the types and strength of hydrogen trap sites, the present approach can predict the fracture resistance of hydrogen charged samples.

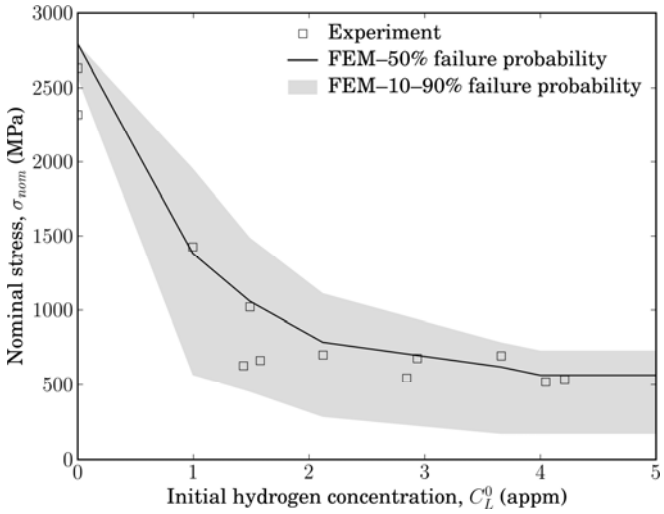

Figure 7. Nominal stress at failure probability $\Phi = 50\%$ denoted by the solid line. The grey region denotes the stress necessary to achieve failure probabilities ranging from 10 to 90%.

5. Summary and Conclusions

We presented a model for hydrogen transport that accounts for trapping of hydrogen at microstructurar defects and addresses the interaction of hydrogen solute atoms with material deformation. In the case of low strength pipeline steels, we found that constraint fracture mechanics can be used to ascertain the behavior of an axial crack in the ID surface of the pipe. The transport model combined with the micromechanism of decohesion in a statistical fracture model provides a reliable means of assessing the fracture resistance of high strength steels to hydrogen degradation.

Acknowledgments

The authors gratefully acknowledge support from (i) U.S. Department of Energy Grant GO15045; (ii) National Science Foundation Grant DMR 0302470; and (iii) the NEDO Project “Fundamental Research Project on Advanced Hydrogen Science” (2006-2012).

References:

[1] J.P. Hirth, Effect of hydrogen on the properties of iron and steel, Metall Trans A 11(6) (1980) 861-890
[2] D.S. Shih, I.M. Robertson, H.K. Birnbaum, Hydrogen embrittlement of α titanium: in situ TEM studies, Acta Metall, 36, (1988) 111-124
[3] H.K. Birnbaum, I.M., Robertson, P. Sofronis P., D. Teter, Mechanisms of hydrogen related fracture—a review, in: T. Magnin (Ed.) Corrosion Deformation Interactions CDI'96 (Second International Conference, Nice, France, 1996), The Institute of Materials, Great Britain, 1997, pp. 172-195
[4] R.A. Oriani, P.H. Josephic, Equilibrium aspects of hydrogen-induced cracking of steel, Acta Metall, 22, (1974) 1065-1074
[5] D.M. Parks, Advances in characterization of elastic-plastic crack-tip fields, A.S. Argon (Ed.), in: Topics in Fracture and Fatigue, Springer-Verlag, Berlin, 1992, pp. 59-98
[6] P. Sofronis, R.M. McMeeking, Numerical analysis of hydrogen transport near a blunting crack tip, J Mech Phys Solids 37(3) (1989) 317-350
[7] R.A. Oriani, The diffusion and trapping of hydrogen in steel, Acta Metall 18 (1970) 147-157
[8] A.H.M. Krom, R.W.J. Koers, A. Bakker, Hydrogen transport near a blunting crack tip, J Mech Phys Solids 47(4) (1999) 971-992
[9] M. Dadfarnia, B.P. Somerday, P. Sofronis, I.M. Robertson, On the small scale character of the stress and hydrogen concentration fields at the tip of an axial crack in steel pipeline: effect of hydrogen-induced softening on void growth, Int J Mater Res 99(5) (2008) 557-570
[10] M. Dadfarnia, B.P. Somerday, P. Sofronis, I.M. Robertson, D. Stalheim, Interaction of hydrogen transport and material elastoplasticity in pipeline steels, J Press Vessel Tech, In print (2008)
[11] A.J. Kumnick, H.H. Johnson, Deep trapping states for hydrogen in deformed iron, Acta Metall 28(1) (1980) 33-39
[12] M. Dadfarnia, P. Sofronis, B.P. Somerday, I.M. Robertson, Effect of remote hydrogen boundary conditions on the near crack-tip hydrogen concentration profiles in a cracked pipeline: fracture toughness assessment, in: Proc of Materials Innovations in an Emerging Hydrogen Economy (Hydrogen 2008), Cocoa Beach, Florida, USA (February 2008)
[13] C.J. McMahon Jr., Hydrogen-induced intergranular fracture of steels, Eng Fract Mech 68 (2001) 773-788
[14] J.P. Hirth, J.R. Rice, On the thermodynamics of adsorption at interfaces as it influences decohesion, Metall Trans A 11(9) (1980) 1501-1511
[15] T. Lin, A.G. Evans, R.O. Ritchie, A statistical model of brittle fracture by transgranular cleavage, J Mech Phys Solids, 34 (1986) 477-497
[16] E. Smith, The nucleation and growth of cleavage microcracks in mild steel, in: A.C Stickland, Proc. Conf. Physical Basis of Yield and Fracture, Inst Phys Phys Soc, Oxford, 1966, pp. 36-48
[17] Y. Liang, P. Sofronis, Toward a phenomenological description of hydrogen-induced decohesion at particle/matrix interfaces, J Mech Phys Solids, 51 (2003) 1509-1531